Ab initio Prediction of Martensitic and Intermartensitic Phase Boundaries in Ni-Mn-Ga

B. Dutta,[1,*] A. Çakır,[2] C. Giacobbe,[3] A. Al-Zubi,[1,†] T. Hickel,[1] M. Acet,[4] and J. Neugebauer[1]
[1]*Max-Planck-Institut für Eisenforschung GmbH, D-40237 Düsseldorf, Germany*
[2]*Muğla Üniversitesi, Metalurji ve Malzeme Mühendisliği Bölümü 48000 Muğla, Turkey*
[3]*European Synchrotron Research Facility, 38043 Grenoble Cedex 9, France*
[4]*Experimentalphysik, Universität Duisburg-Essen, D-47048 Duisburg, Germany*
(Received 8 June 2015; published 15 January 2016)

Despite the importance of martensitic transformations of Ni-Mn-Ga Heusler alloys for their magnetocaloric and shape-memory properties, the martensitic part of their phase diagrams is not well determined. Using an *ab initio* approach that includes the interplay of lattice and vibrational degrees of freedom we identify an intermartensitic transformation between a modulated and a nonmodulated phase as a function of excess Ni and Mn content. Based on an evaluation of the theoretical findings and experimental x-ray diffraction data for Mn-rich alloys, we are able to predict the phase diagram for Ni-rich alloys. In contrast to other mechanisms discussed for various material systems in the literature, we herewith show that the intermartensitic transformation can be understood solely using thermodynamic concepts.

DOI: 10.1103/PhysRevLett.116.025503

The Ni-Mn-based Heusler systems are of great interest due to the observation of extraordinary large magnetic shape-memory effects (MSMEs) and magnetocaloric effects (MCEs). Any application of these important properties requires the detailed knowledge of their composition-temperature phase diagrams and control of the underlying phase transformations: The MSME relies on recoverable strains during the martensitic transformation of up to 10% [1] that can only be achieved by certain martensitic phases. Furthermore, transformation temperatures above room temperature are needed for applications as actuators. The MCE requires a coupling of a magnetic transition to the first-order structural transformation to achieve entropy changes that are sufficient for cooling applications. Again, this constraint is only fulfilled in certain composition ranges and the efficiency strongly depends on the crystal structure of the martensitic phase.

Indications for this chemical sensitivity come from experiments: dependent on the composition, the martensitic transformations from a parent cubic $L2_1$ structure result in various product nonmodulated $L1_0$ and modulated martensitic phases [2–4]. The modulated variants can be commensurate ($5M_C$) or incommensurate ($5M_{IC}$, $7M_{IC}$), sinusoidal or twinned [5,6]. Ongoing debates about whether their origin is phonon softening [7,8], structural adaptation to accommodate the lattice mismatch to the austenite [9], or connection to magnetic ordering [6] demonstrate the physical appeal of these investigations. A new and exciting observation has the potential to complicate and/or clarify the situation: due to recently encountered intermartensitic transformations even two martensitic phases are for the same composition possible [3,10,11]. Such a phenomenon is not restricted to Heusler alloys, and multistage martensitic transitions and modulations of structures have also been observed in Ni-Ti alloys [12,13], $Fe_{70}Pd_{30}$ [14], Ni-Al alloys [15], and others [16,17].

Our own experimental work allowed us to look at chemical trends for the intermartensitic transformation temperature T_{IM} [4] in Ni-Mn-Ga alloys. We made the interesting observation that the structure with the seemingly higher symmetry ($L1_0$) tends to be more stable in the ground state than modulated phases (Fig. 2). Further, the $L1_0$ phase seems to dominate those regions of the phase diagram that are due to the high martensitic transformation temperatures T_M particularly interesting for the MSME and MCE. In contrast to the narrow hysteresis at T_M, these intermartensitic transformations involve a large hysteresis of about 100 K. Since both the presence of the $L1_0$ phase and large hysteresis effects hamper the applicability of the material, it is important to manage the intermartensitic transformations.

Conclusions solely from experiment are limited by the fact that $L1_0$ is rarely a pure phase, but is mixed with modulated phases. Furthermore, our previous measurements were restricted to a narrow range of samples with increased Mn content, $Ni_2Mn_{1+y}Ga_{1-y}$, while an increased Ni content, $Ni_{2+x}Mn_{1-x}Ga$, is equally important for applications, but has been much less systematically investigated. For a generalization and connection of both regimes, it is decisive to know whether control parameters like the averaged electron concentrations per atom (e/a) [18], which work well for T_M, can also be applied to T_{IM}.

To resolve these open issues, we introduce *ab initio* methods to derive the phase diagram of Ni-Mn-Ga. A purely theoretical prediction of composition-temperature-dependent phase diagrams is challenging, since (i) dense screening of chemical variations is required, (ii) the configuration space is large due to broken symmetry,

(iii) energy differences are in the order of a few meV/atom, and (iv) tiny effects such as magnetic modifications can therefore become decisive. In previous *ab initio* works [19,20], off-stoichiometric Heusler alloys were screened by using total energy differences between the $L2_1$ and $L1_0$ structures as an estimate for T_M. Since vibrational, configurational, and magnetic excitations are not considered, the approach is not able to resolve the temperature-dependent competition of modulated and nonmodulated phases that is essential for intermartensitic transitions.

Going beyond this approach requires the combination of density functional theory with thermodynamic concepts for all excitation processes contributing to the entropy. Because of the principle limitations of exchange-correlation (xc) functionals, it is *a priori* unclear if reliable transformation temperatures can be achieved. Previous studies showed that a precision of free energies below 1 meV/atom is feasible for quasiharmonic [21] and anharmonic [22,23] entropy contributions. Furthermore, we have shown [24] that the Perdew-Burke-Ernzerhof xc functional [25] yields for stoichiometric Ni_2MnGa a very good description of the sequence of phase transitions, if the delicate interplay of vibrational and magnetic degrees of freedom is employed. Following this strategy, the vibrational contributions are also in the present work determined within the quasiharmonic approximation [26]. The magnetic excitations below the Curie temperature are taken into account in a fixed-spin moment approach. The Curie temperatures T_C used for this are taken from experiments [2,3,27] (Fig. 2) for the austenite and are results of Monte Carlo simulations [28] for the martensitic phases.

The calculations with the VASP package [29] are performed in unit cells elongated along the [110] direction with respect to the conventional fcc unit cell to capture the $L2_1$ austenite (24 atoms), the $L1_0$ martensite (24 atoms), but also the commensurate modulated $5M_C$ (40 atoms) and $7M_C$ (56 atoms) structures. Following experiments, sinusoidal atomic shifts were assumed for the $5M_C$ structure, whereas the $7M_C$ structure was considered in a $5\bar{2}$ twinned configuration [9]. For the sake of clarity, we exclude the $3M$ structure from the discussion.

Examples for the obtained free energies are shown in Fig. 1. In the stoichiometric case of Ni_2MnGa the relation between the austenitic $L2_1$ phase (orange) and the nonmodulated ($L1_0$) martensitic phase (green, reference structure) is consistent with our earlier findings (Fig. 4 in Ref. [24]). Evaluating these two phases only, a martensitic transformation at 182 K would be expected. The sinusoidal $5M_C$ phase (not computed in Ref. [24]) has at the stoichiometric composition for low temperatures a larger free energy than the $L1_0$ martensite. At higher temperatures it gains vibrational entropy compared to $L1_0$ and becomes thermodynamically stable. A second intersection occurs at 292 K, fulfilling the expectation that the structure with higher symmetry eventually dominates. It turns out,

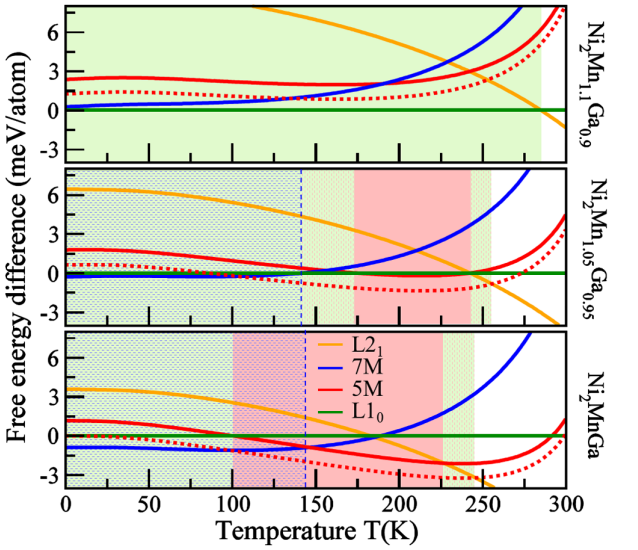

FIG. 1. Calculated free energies of the $L2_1$ (orange lines), $5M$ (red), and $7M$ (blue) phases relative to the respective $L1_0$ (green) martensitic phase for three (given) compositions. The red dotted line represents a shift of the $5M$ free energy after adaptation to experiment for Ni_2MnGa. The background colors indicate phase stabilities (compare Fig. 3).

however, that the latter transformation is mainly due to the difference in T_C of the two martensitic phases, i.e., of magnetic origin (compare Ref. [6]). The low-temperature sequence of phase transformations can only be fully understood by noting that $5M_C$ and $L1_0$ are not connected by a barrier-free transformation path (soft phonons), but belong to different energy minima (different c/a ratios) on the complex energy landscape.

The situation is comparable for the $7M_C$ phase, the second new phase of this Letter, though its $5\bar{2}$ twinned configuration qualitatively distinguishes the structure from sinusoidal $5M_C$. Its structure is similar to $L1_0$, but its energy at $T = 0$ K is lower due to slightly negative twin-boundary energies, in particular for $X\bar{2}$ (X integer) configurations [30]. The vibrational entropy turns out to be almost identical to that of the $L1_0$ phase. This behavior depends, however, very critically on the choice of T_C for $7M_C$, for which we have chosen (as for $5M_C$) the value for an orthorhombic structure with $c/a = 0.93$ [28].

The off-stoichiometric results will first be discussed for $Ni_2Mn_{1+y}Ga_{1-y}$. Here, we can evaluate the predicted chemical trends for T_M as well as T_{IM}, since experimental data are available. Off-stoichiometric (Mn-rich) compositions have been achieved by considering one Mn antisite per supercell. In the case of 24 (40, 56) atomic supercells, this corresponds to an excess Mn content of $y = 0.166$ (0.10, 0.07) on the Ga sublattice. In some cases, the broken symmetry requires the consideration of configurational entropy: it is equal for $L2_1$ and $L1_0$, but can be different for the modulated structures, since antisites prefer undisplaced instead of arbitrary lattice sites.

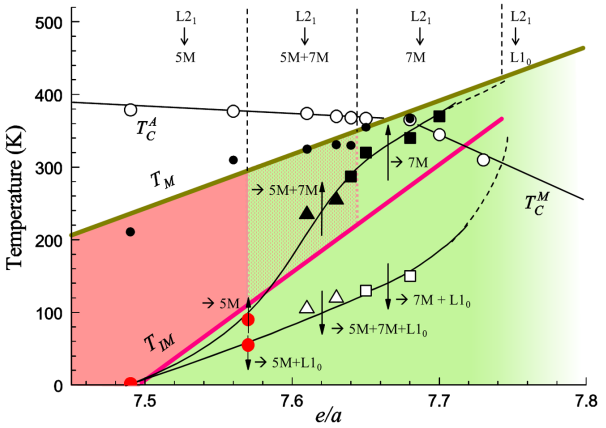

FIG. 2. Experimental phase diagram for $Ni_2Mn_{1+y}Ga_{1-y}$. Open circles represent Curie temperatures in austenite (T_C^A) and martensite (T_C^M). Filled circles indicate the martensitic transition T_M (fitted by the green line). Intermartensitic transition temperatures are shown with open (forward) and filled (reverse transformation) squares (for $7M \leftrightarrow 7M + L1_0$) and triangles (for $5M + 7M \leftrightarrow 5M + 7M + L1_0$), respectively (compare Ref. [4]). New data points are plotted as red circles. The red line estimates the equilibrium intermartensitic transition boundary T_{IM}: Below the line, phase fractions of $L1_0$ are observed (green-colored area); above the line only $5M$ (red colored), a mixture of $5M$ and $7M$ (red textured), or only $7M$ (green colored) is observed.

There is no principle problem with directly calculating phase transformations for other Mn concentrations, but it involves a huge computational demand. We have therefore employed an interpolation scheme for the construction of the phase diagrams. Following the philosophy of CALPHAD [31], we consider the free energy $F^\sigma(x,T)$ of the individual phases σ as the central quantity, for which we assume a polynomial (linear) dependence on the concentration x:

$$F^\sigma(x,T) = \frac{x_1 - x}{x_1 - x_0} F^\sigma(x_0,T) + \frac{x - x_0}{x_1 - x_0} F^\sigma(x_1,T). \quad (1)$$

Here, x_0 is the stoichiometric and x_1 the second (phase dependent) concentration, for which *ab initio* free energies have been determined.

The physical results for $Ni_2Mn_{1.1}Ga_{0.9}$ are qualitatively different from the stoichiometric behavior: now the modulated structures are thermodynamically not stable and a direct phase transformation between austenite and $L1_0$ occurs at $T_M = 285$ K. In order to describe the transition between both cases and resolve the critical Mn concentration, we determine free energies for other (interpolated) compositions such as $Ni_2Mn_{1.05}Ga_{0.95}$ (Fig. 1). This is close to the critical concentration for the presence of $5M$ and characterizes the onset of a second stability region of $L1_0$ below T_M at 242 K.

The full phase diagram for $Ni_2Mn_{1+y}Ga_{1-y}$ is shown in Fig. 3(a). We discuss these findings in comparison with the experimental data shown in Fig. 2. To better recognize the common features, the T_M and T_{IM} boundaries in Fig. 2 have been copied into Fig. 3 and identical shading has been introduced. The most important success of the *ab initio* calculations is the prediction of the austenite-martensite transformation temperature T_M [32,33]. The deviations of the absolute values are approximately 30 K, but the chemical trends of our and other experiments [27,34–36] are perfectly reproduced.

For the discussion of the martensitic region, we first focus on the sinusoidal $5M_C$ phase (red), since it can be structurally and energetically much better distinguished from the competing $L1_0$ phase (green) than the twinned $7M$ phase. The observed large stability region of $5M_C$ is in agreement with experiments [34,36–38], where it is for several $Ni_2Mn_{1+y}Ga_{1-y}$ alloys established that the

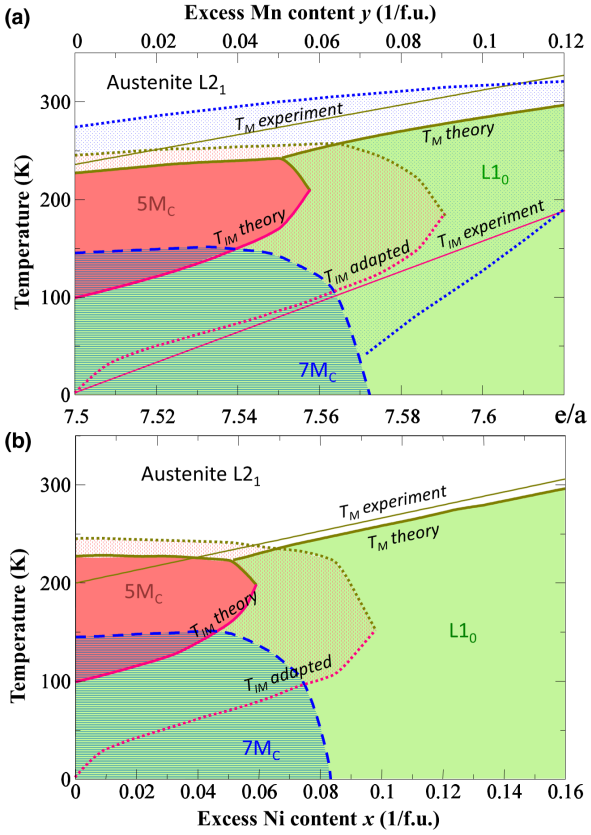

FIG. 3. *ab initio* calculated phase diagram of (a) $Ni_2Mn_{1+y}Ga_{1-y}$ and (b) $Ni_{2+x}Mn_{1-x}Ga$. The martensitic transformation T_M (thick green line) separates the austenite from different martensitic phases. The intermartensitic transformation T_{IM} (thick red line) occurs between the $5M_C$ (red-colored area) and the $L1_0$ phase (green-colored). For comparison, linear fits for T_M and T_{IM} as taken from (a) Fig. 2 and (b) Ref. [27] are shown by thin lines. The red-textured area shows the extension of the $5M$ stability region, if its free energy at the stoichiometric composition is adapated to experimental data. The stability region of $7M_C$ is indicated by a blue dashed line with a numerical uncertainty given by blue dotted lines (see text).

austenite-martensite transition in a cooling process will first yield $5M$ (Fig. 2). With the present work we confirm that the phase is thermodynamically stable and not the result of an adaptation to the lattice constant of austenite [9].

The highest Mn content for which $5M_C$ is observed in the *ab initio* phase diagram corresponds to $e/a = 7.55$. Consequently, $L1_0$ dominates the martensite in a rather large composition region, including Mn contents that are due to the high T_M values interesting for applications. The finding is again in good agreement with our experiments, where the boundary for the sole presence of $5M$ is $e/a = 7.57$. The intermartensitic transition between the $5M$ and the $L1_0$ phase is displayed by solid red lines in Figs. 2 and 3. The *ab intio* calculations indicate that $L1_0$ is at the ground state more stable than the sinusoidal $5M$ phase throughout the considered compositions. This is an important confirmation of the experimental findings.

The definition of a sharp boundary between both phases is, however, not straightforward. First, the experimental phase diagram in Fig. 2 contains a red-textured region where mixtures of $5M$ and $7M$ are observed. Second, the experiment experiences large hysteresis effects, and only a linear interpolation of the equilibrium T_{IM} (averaged forward and reverse transformation) is plotted (compare Ref. [10]). Third, an error bar in the *ab initio* determination of T_{IM} similar to T_M should be incorporated. We consider the stoichiometric composition to be most suitable for adjustments. Since experimental data for T_{IM} were only available for $e/a > 7.6$, it was important to achieve new measurements (red points in Fig. 2) down to the stoichiometric composition. They were carried out at the ID22 high resolution diffractometer beam line at the European Synchrotron Research Facility in Grenoble, France for the compositions $Ni_{49.8}Mn_{25.0}Ga_{25.2}$ ($e/a = 7.49$) and $Ni_{49.8}Mn_{27.1}Ga_{23.1}$ ($e/a = 7.57$). To investigate hysteresis effects, samples have first been cooled down to 10 K and afterwards warmed to room temperature again. Rietveld refinements have been performed for temperature steps of 10 K using Fullprof [39] and Jana2000 [40]. To identify the presence of the $L1_0$ phase, (112) and (200) reflections have been particularly considered (see Ref. [4] for more details).

The new experimental data are in agreement with the theoretically predicted continuation of the phase boundary down to the stoichiometric composition ($e/a = 7.5$). The quantitative values for T_{IM} (linear fit in Fig. 2), however, are lower than in theory. The dotted red line in Fig. 3 indicates that a free-energy adjustment for the modulated $5M_C$ phase by 1.13 meV/atom (to match experiment at $e/a = 7.5$) improves the agreement to the experimental T_{IM} over the whole composition range. Consequently, the stability region of $5M_C$ increases (red-textured area), while the qualitative features of the phase diagram remain unchanged.

We now extend the discussion to twinned $7M$ martensite, which is structurally similar to nonmodulated $L1_0$. Consequently, it is difficult to distinguish both phases (tiny energy differences in Fig. 1). In particular, a change of T_C can change the stability: choosing the same T_C as $5M$ (similar c/a ratio, most likely scenario) yields the blue dashed line, while the same T_C as $L1_0$ (similar crystal structure, extreme scenario) yields the blue dotted line. According to the first scenario, the $5M_C$ structure directly transforms into this $7M_C$ phase and a phase boundary between the austenite and the $7M$ phase is not observed. In the second scenario, the $7M$ phase can be stable in a large region of the martensite and will have a direct phase boundary to the austenite. Independent of this choice, the $L1_0$ phase is the ground state in a certain region of the phase diagram, but not at the stoichiometric composition. The presence of the $7M$ phase close to stoichiometry in synchrotron experiments is currently under debate. It was not possible to undoubtedly verify it in our measurements (Fig. 2), whereas other groups claim to observe it [8]. Note that the consideration of incommensurate $7M_{IC}$ structures as reported there would yield an even larger stability region of $7M$ in the phase diagram.

Based on the evaluation of the *ab initio*–based phase diagram for $Ni_2Mn_{1+y}Ga_{1-y}$ we are now confident to achieve reliable predictions for $Ni_{2+x}Mn_{1-x}Ga$ [Fig. 3(b)]. These two material systems differ apart from the chemistry also in their magnetic properties and atomic relaxations next to the antisite atoms. Having this in mind, the two phase diagrams in Fig. 3 are remarkably similar. This applies to the overall topology as well as to the quantitative values for the critical compositions and temperatures for the intermartensitic transformations.

The differences are apparently compensated by similar electronic properties in Ni-rich and Mn-rich alloys, as expressed by the electron concentration per atom e/a. We can conclude that this parameter is not only suitable for the determination of T_M (supported by experiment [27]), but also for T_{IM}. This gives further confidence in the reliability of the *ab initio* phase diagram and in particular the chemical trend for T_{IM} obtained for $Ni_{2+x}Mn_{1-x}Ga$ [Fig. 3(b)]. Regarding quantitative values, we apply again an adaptation of our *ab initio* results for the $5M$ phase, since Fig. 3(b) has the stoichiometric composition ($e/a = 7.5$) in common with Fig. 3(a).

In conclusion, we have extended *ab initio* concepts towards the full derivation of composition-temperature phase diagrams. This gave access to valuable insights about the origin of the transformations in martensitic phases currently debated in the literature. Using the example of $Ni_2Mn_{1+y}Ga_{1-y}$ we clarify that sinusoidal modulated phases (here $5M$) can be thermodynamically stable in certain composition ranges, without the need of an adaptation to the austenite or precursor effects. Martensitic structures with higher symmetry (here $L1_0$) can still serve as the ground state, if they are not connected by a barrier-free transformation to the modulated phase. The stability of

twinned structures (here 7*M*) is more difficult to identify, since the resulting entropy changes are negligible. While we limited the extension of the theoretical concepts to $Ni_{2+x}Mn_{1-x}Ga$, similar rules should also apply to other material systems relevant for the MSME and the MCE.

We would like to acknowledge Dr. M. Gruner, Professor P. Entel, and Dr. S. Singh for fruitful discussions, and the Deutsche Forschungsgemeinschaft (DFG) for their funding within the priority program (SPP1599).

*b.dutta@mpie.de
†Present address: American University of the Middle East, College of Engineering and Technology, 54200 Egaila, Kuwait.

[1] A. Sozinov, A. A. Likhachev, and K. Ullakko, IEEE Trans. Magn. **38**, 2814 (2002).
[2] X. Xu, M. Nagasako, W. Ito, R. Y. Umetsu, T. Kanomata, and R. Kainuma, Acta Mater. **61**, 6712 (2013).
[3] Z. Li, N. Xu, Y. Zhang, C. Esling, J.-M. Raulot, X. Zhao, and L. Zuo, Acta Mater. **61**, 3858 (2013).
[4] A. Cakir, L. Righi, F. Albertini, M. Acet, M. Farle, and S. Aktürk, J. Appl. Phys. **114**, 183912 (2013).
[5] L. Righi, F. Albertini, S. Fabricci, and A. Paoluzi, Mater. Sci. Forum **684**, 105 (2011).
[6] S. O. Mariager, T. Huber, and G. Ingold, Acta Mater. **66**, 192 (2014).
[7] A. Zheludev, S. M. Shapiro, P. Wochner, and L. E. Tanner, Phys. Rev. B **54**, 15045 (1996).
[8] S. Singh, V. Petricek, P. Rajput, A. H. Hill, E. Suard, S. R. Barman, and D. Pandey, Phys. Rev. B **90**, 014109 (2014).
[9] S. Kaufmann, U. K. Rößler, O. Heczko, M. Wuttig, J. Buschbeck, L. Schultz, and S. Fähler, Phys. Rev. Lett. **104**, 145702 (2010).
[10] L. Straka, A. Sozinov, J. Drahokoupil, V. Kopecky, H. Hänninen, and O. Heczko, J. Appl. Phys. **114**, 063504 (2013).
[11] C. Seguí, V. A. Chernenko, J. Pons, E. Cesari, V. Khovailo, and T. Takagi, Acta Mater. **53**, 111 (2005).
[12] N. A. Zarkevich and D. D. Johnson, Phys. Rev. Lett. **113**, 265701 (2014).
[13] Y. Ji, D. Wang, X. Ding, K. Otsuka, and X. Ren, Phys. Rev. Lett. **114**, 055701 (2015).
[14] A. Arabi-Hashemi and S. G. Mayr, Phys. Rev. Lett. **109**, 195704 (2012).
[15] S. M. Shapiro, B. X. Yang, G. Shirane, Y. Noda, and L. E. Tanner, Phys. Rev. Lett. **62**, 1298 (1989).
[16] Y. Sutou, Y. Imano, N. Koeda, T. Omori, R. Kainuma, K. Ishida, and K. Oikawa, Appl. Phys. Lett. **85**, 4358 (2004).
[17] R. F. Hamilton, H. Sehitoglu, C. Efstathiou, and H. J. Maier, Acta Mater. **55**, 4867 (2007).
[18] V. A. Chernenko, E. Cesari, V. V. Kokorin, and I. N. Vitenko, Scr. Mater. **40**, 523 (1999).
[19] P. Entel, V. D. Buchelnikov, M. E. Gruner, A. Hucht, V. V. Khovailo, S. K. Nayak, and A. T. Zayak, Mater. Sci. Forum **583**, 21 (2008).
[20] M. Siewert *et al.*, Appl. Phys. Lett. **99**, 191904 (2011).
[21] B. Grabowski, T. Hickel, and J. Neugebauer, Phys. Rev. B **76**, 024309 (2007).
[22] B. Grabowski, P. Söderlind, T. Hickel, and J. Neugebauer, Phys. Rev. B **84**, 214107 (2011).
[23] A. Glensk, B. Grabowski, T. Hickel, and J. Neugebauer, Phys. Rev. Lett. **114**, 195901 (2015).
[24] M. A. Uijttewaal, T. Hickel, J. Neugebauer, M. E. Gruner, and P. Entel, Phys. Rev. Lett. **102**, 035702 (2009).
[25] J. P. Perdew, K. Burke, and M. Ernzerhof, Phys. Rev. Lett. **77**, 3865 (1996).
[26] J. Xie, S. de Gironcoli, S. Baroni, and M. Scheffler, Phys. Rev. B **59**, 965 (1999).
[27] A. N. Vasilev, A. D. Bozhko, V. V. Khovailo, I. E. Dikshtein, V. G. Shavrov, V. D. Buchelnikov, M. Matsumoto, S. Suzuki, T. Takagi, and J. Tani, Phys. Rev. B **59**, 1113 (1999).
[28] P. Entel, A. Dannenberg, M. Siewert, H. C. Herper, M. E. Gruner, D. Comtesse, H.-J. Elmers, and M. Kallmayer, Metall. Mater. Trans. A **43**, 2891 (2012).
[29] G. Kresse and J. Furthmüller, Phys. Rev. B **54**, 11169 (1996).
[30] M. Gruner *et al.* (unpublished).
[31] N. Saunders and A. P. Miodownik, *CALPHAD (Calculation of Phase Diagrams): A Comprehensive Guide* (Pergamon, Oxford, 1998).
[32] T. Hickel, M. Uijttewaal, A. Al-Zubi, B. Dutta, B. Grabowski, and J. Neugebauer, Adv. Eng. Mater. **14**, 547 (2012).
[33] B. Dutta, T. Hickel, P. Entel, and J. Neugebauer, J. Phase Equilib. Diffus. **35**, 695 (2014).
[34] R. Ranjan, S. Banik, S. R. Barman, U. Kumar, P. K. Mukhopadhyay, and D. Pandey, Phys. Rev. B **74**, 224443 (2006).
[35] F. Albertini, A. Paoluzi, L. Pareti, M. Solzi, L. Righi, E. Villa, S. Besseghini, and F. Passaretti, J. Appl. Phys. **100**, 023908 (2006).
[36] N. Lanska, O. Söderberg, A. Sozinov, Y. Ge, K. Ullakko, and V. K. Lindroos, J. Appl. Phys. **95**, 8074 (2004).
[37] P. Lázpita, J. M. Barandiarán, J. Gutiérrez, M. Richard, S. M. Allen, and R. C. O'Handley, Eur. Phys. J. Spec. Top. **158**, 149 (2008).
[38] Z. Li, Y. Zhang, C. Esling, X. Zhao, and L. Zuo, Acta Mater. **59**, 3390 (2011).
[39] J. Rodriguez-Carvajal, Physica (Amsterdam) **192B**, 55 (1993).
[40] V. Petricek, M. Dusek, and L. Palatinus, Z. Kristallogr. **229**, 345 (2014).